# High-magnetic-field study of magnetic and transport properties of hole-doped $NdBaCo_2O_{5+\delta}$

E. S. Vlakhov,[1,5,*] N. Kozlova,[2] L. S. Lobanovskii,[3] R. Wawryk,[4] and K. A. Nenkov[2,5]

[1]*Institute of Solid State Physics, Bulgarian Academy of Sciences, 72 Tzarigradsko Chaussee Boulevard, 1784 Sofia, Bulgaria*

[2]*Leibnitz Institut für Festkörper- und Werkstofforschung Dresden, D-01171, Dresden, Germany*

[3]*Joint Institute of Solid State Physics and Semiconductor Physics, National Academy of Sciences of Belarus, Minsk, 220072, Belarus*

[4]*Institute of Low Temperature and Structure Research, Polish Academy of Sciences, 50-950 Wrocław, Poland*

[5]*International Laboratory for High Magnetic Fields and Low Temperatures, 95 Gajowicka Street, 53-421 Wrocław, Poland*

(Received 28 June 2011; revised manuscript received 10 November 2011; published 30 November 2011)

Magnetic and transport properties of the $NdBaCo_2O_{5+\delta}$ system are studied in the less investigated hole-doped region ($0.52 < \delta < 0.72$) and in pulsed magnetic fields up to 47 T. The conductance in zero-magnetic field and $T < 130$ K is described by a two-gap expression completed by the term of variable range hopping (VRH). The thermoelectric power $S(T)$ measurements confirm the magnetic phase diagram found by magnetic and electric transport investigations. It has been shown that ferromagnetic behavior of $NdBaCo_2O_{5+\delta}$ ($0.52 < \delta < 0.72$) is stabilized and spans in lower temperatures by increasing the external magnetic field in agreement with structural and magnetic phase diagrams found on the $NdBaCo_2O_{5.75}$ and $GdBaCo_2O_{5+\delta}$ systems. Variable range hopping mode gives good approximation in zero- and high-magnetic field 47 T. The isothermal magnetoconductance ($G$) of hole-doped polycrystalline $NdBaCo_2O_{5.72}$ is well fitted by $G(H,T)/G(0) = G_0\exp(H/H_0)$ dependence at 55 K $< T <$ 138 K (the region where FM state appears) instead of simple linear dependence found for manganites $La_{0.7}Sr_{0.3}MnO_3$. The parameter $H_0$ is considered as the magnetic field of full spin sublattices' reorientation and *MR* saturation. The magnetoconductance is possibly realized through the *a*-oriented grains due to the strong decrease of resistivity $\Delta\rho_c/\rho_c$ in magnetic field along the *a* axis. The deduced reason for observed behavior is the specific origin of the antiferromagnetic (AFM)-ferromagnetic (FM) transition in layered cobaltites.

DOI: 10.1103/PhysRevB.84.184440 PACS number(s): 75.50.Dd, 75.47.Lx, 64.75.Jk, 72.20.Pa

## I. INTRODUCTION

Perovskites with typical formulae $RBO_3$ (where $R$ is a rare earth element and $B$ is a transition metal such as Cu, Mn, Ni, Co, Ti, Ru, etc.) have been intensively investigated worldwide for decades. The motivation is their prototypical behavior and spectacular functionality, like high-temperature superconductivity (cuprates), ferroelectricity (titanates), colossal magnetoresistance (manganites), etc. Extraordinary properties of transition-metal oxides have been implemented in new functionality devices and innovation technology. $RBaCo_2O_{5+\delta}$ compounds ($R$ = rare earth) consist of consecutive ordered square-lattice layers $(CoO_2)$-(BaO)-$(CoO_2)$-$(RO_x)$ stacked along the perovskite $c$ axis. It has been found that weak change of electrical, magnetic, or lattice parameters of $RBaCo_2O_{5+\delta}$ compounds results in drastic change of their behavior.[1–12] They have been used to investigate an additional degree of freedom introduced by the ability of $Co^{+3}$ ions to exist in three different spin states: the low-spin state (LS, $t_2{}^6\ e_g{}^0$, $S = 0$), intermediate-spin state (IS, $t_{2g}{}^5\ e_g{}^1$, $S = 1$), and the high-spin state (HS, $t_{2g}{}^4\ e_g{}^2$, $S = 2$).[13] Due to small energy gaps between these states, the LS evolves to the IS and then to the HS as the temperature increases. Except the thermal excitations, the change in the local crystal environment of the cobalt ions can transform them, too, from one spin state to another, thus resulting in the appearance of different spin structures, spin-state ordering transitions, and complex magnetic phase diagram.[10,14] Cobaltites $RBaCo_2O_{5+\delta}$ have been extensively characterized worldwide (Europe, USA, Japan, Australia, etc.) employing modern and heavy scientific infrastructure as resonant soft and hard x-ray diffraction, neutron powder diffraction, muon spin polarization, synchrotron radiation, pulsed high magnetic fields, etc.[4,6,9,15–21] Beyond spectacular low-temperature magnetotransport behavior (found at $T <$ 400 K) $RBaCo_2O_{5+\delta}$ possess additional very useful properties, like high chemical stability, good oxygen permeability, and mixed electronic and ionic conductance at higher temperature range (500–700 °C).[22–26] This complex of properties makes cobaltites suitable material for energy conversion; however, a few studies on thin cobaltite films deposition and characterization are known.[27–31]

Very important features of $RBaCo_2O_{5+\delta}$ compounds are a wide range of doping ($0 < \delta < 1$) and the possibility of reversible tuning of $\delta$ by oxygen partial pressure. It has been found that $\delta$ depends on the size of the rare earth element $R$ in polycrystalline compounds sintered in air: the larger the size of $R$ is, the larger oxygen stoichiometry is reached.[2] Doping by oxygen influences strongly the Co ion coordination (octahedral or pyramidal) and thus the Co spin state and magnetic and transport properties of the $RBaCo_2O_{5+\delta}$ compounds. Comprehensive investigations of Taskin *et al.*[10–12] on single crystals of $GdBaCo_2O_{5+\delta}$ and $NdBaCo_2O_{5+\delta}$ systems have been carried out employing fine oxygen stoichiometry tuning. As a result, a detailed magnetic phase diagram in the temperature region 4 K $< T <$ 400 K has been proposed. After these authors, the properties of three compounds with oxygen stoichiometry $\delta = 0$, $\delta = 0.50$, and $\delta \sim 0.70$ are of profound importance (prototypical) because they underline the behavior of compounds with intermediate oxygen stoichiometry (see Fig. 20 of Ref. 10).

The prototypical composition with $\delta = 0.50$ has attracted much attention, resulting in the discovery of complex types of spin ordering.[4,6,9,10,19,21,24,32,33] Using muon spin resonance technique, Luetkens *et al.*[15] and Jarry *et al.*[16] have found that complicated magnetic behavior of $RBaCo_2O_{5.50}$ ($R$ = Y, Tb,

 

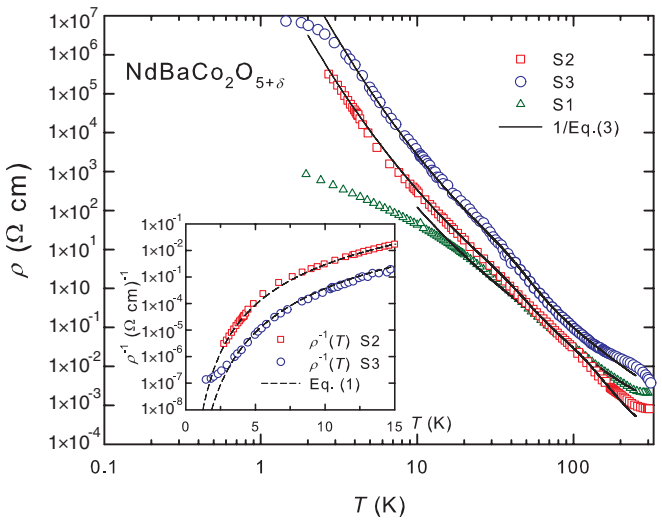


FIG. 1. (Color online) Electrical resistivity $\rho$ vs temperature $T$ for three samples of $NdBaCo_2O_{5+\delta}$ (S1 = triangles, S2 = squares, and S3 = circles) measured in zero-magnetic field. The solid lines display the data fit by Eq. (3). The dashed lines in the inset represent the data fit to Eq. (1) for samples S2 and S3.

Dy, Ho, and Nd) could be understood in the frame of spin-state ordering (SSO) and phase separation.

The structural and magnetic properties of prototypical composition with $\delta \sim 0.75$ have been investigated for $R = Pr$,[34] $R = Nd$,[7,8,17] and $R = Gd$.[10] In spite of extensive worldwide investigations on layered cobaltites $RBaCo_2O_{5+\delta}$, however, there are few magnetotransport studies that are focused on the oxygen-rich part $0.50 < \delta < 1.00$ of the diagrams. The aim of this paper is to elucidate the magnetic, transport, and magnetotransport properties of the $NdBaCo_2O_{5+\delta}$ system in a relatively less investigated hole-doped region ($0.50 < \delta < 0.72$) and in a wide range of magnetic field up to 47 Tesla.

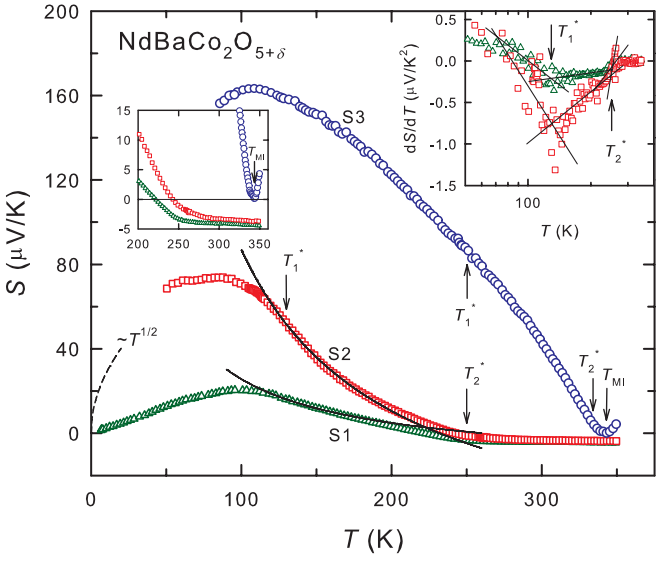


FIG. 2. (Color online) Thermoelectric power vs temperature for three samples of $NdBaCo_2O_{5+\delta}$. The solid lines denote the data fit to Eq. (4). The dashed line displays the hypothetical $S(T)$ dependence for S2 sample. Right inset: the derivative $dS/dT$ vs log $T$ for two samples: S1 (triangles) and S2 (squares). The characteristic temperatures $T_1^*$ and $T_2^*$ are defined in the text. Left inset: details of $S$-vs-$T$ dependence at $T > 200$ K.

## II. EXPERIMENTAL

All investigated polycrystalline samples were obtained by solid-state synthesis of oxides and carbonates of the corresponding elements in two steps. First, the samples were calcined at a temperature of 1,000 °C, then slowly cooled, and finally ground. The synthesis was carried out at a temperature of 1,100 °C. The sample S1 with maximal oxygen stoichiometry $NdBaCo_2O_{5.72}$ (close to that of a prototypical compound $\delta = 0.75$) was obtained by slow cooling in air (at rates less than 20 °C/h) and holding for 24 h at 250 °C (see Refs. 7, 3, and 22). The synthesis of other samples S2 and S3 was carried out in air at higher temperature of 1,200 °C. In order to adjust their oxygen stoichiometry to values $\delta = 0.55$ (sample S2) and $\delta = 0.52$ (sample S3), an additional *ex-situ* annealing in an oxygen environment of 600 Torr has been employed (see Figs. 3 and 4 of Taskin *et al.*[10]). We used a low inert SiC heater mounted in a vacuum chamber of standard VUP-5 set. Ceramic samples were heated up to annealing temperature, held for two hours at this temperature to ensure homogeneous distribution, and quenched (by switching off the heater) to prevent further oxygen uptake.

The electrical resistivity at temperatures of 1.5–310 K was measured by a standard four-point ac method. The setup described by Henkie *et al.*[35,36] was used for the thermoelectric power measurements. The specimens for the measurements of electrical resistivity and thermoelectric power were cut out to the dimensions of about $6 \times 1.5 \times 1$ mm$^3$ and $2.5 \times 0.5 \times 0.5$ mm$^3$, respectively. Magnetization $M(T)$ measurements for $T = 1.9$–400 K and $B = 0$–5.5 T were conducted by using a Quantum Design magnetic properties measurement system or SQ-MPMS-XL7T.

The magnetoresistance measurements have been performed in a pulse-field facility, where magnetic fields up to 50 T were generated by a solenoid.[37] The resistance measurements have been performed using the four-probe technique applying ac current (frequency $f = 10$ kHz).[38] The magnetic-field dependence of the magnetic moment has been measured using a pickup magnetometer.[39]

## III. RESULTS

The temperature dependencies of electrical resistivity, $\rho(T)$ for the three samples (S1, S2, and S3) of $NdBaCo_2O_{5+\delta}$ cobaltite are measured in the temperature range from 2 to 300 K and presented in Fig. 1. The ratios of low temperature resistivity to the resistivity at room temperature, $\rho(2\text{ K})/\rho(300\text{ K})$ are the following: $821/2.1 \times 10^{-3}$, $\sim 6 \times 10^5/8.3 \times 10^{-4}$, and $5.7 \times 10^6/4.7 \times 10^{-3}$ ($\Omega$·cm/$\Omega$·cm) for samples S1, S2, and S3, respectively.

The thermoelectric power, $S$, measured below 350 K down to $T = 6$, 46, and 83 K for samples S1, S2, and S3, respectively is presented in Fig. 2. The values of $S(300\text{ K})/S_{max}/T_{Smax}$ are the following: $-4.1/20.5/100$, $-3.2/73.3/93$, and $42.7/163.5/108$ $\mu$V·K$^{-1}$/$\mu$V·K$^{-1}$/K for samples S1, S2, and S3, respectively.

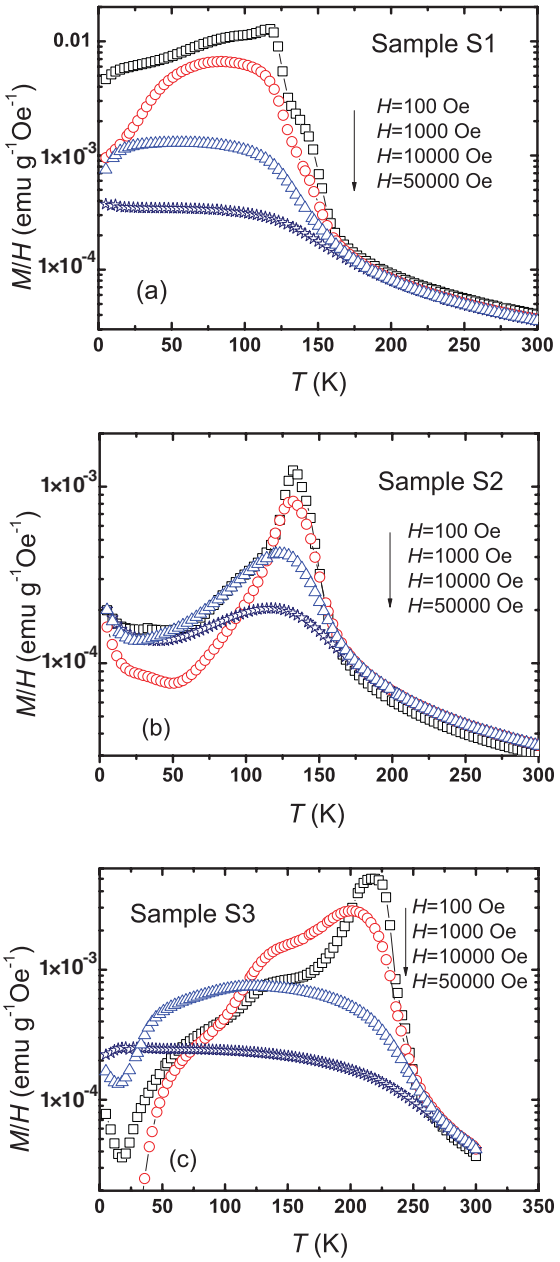


FIG. 3. (Color online) Magnetic susceptibility $\chi = M/H$ vs temperature $T$ for three hole-doped polycrystalline $NdBaCo_2O_{5+\delta}$ samples: (a) S1, (b) S2, and (c) S3, respectively. Data were collected in different magnetic fields $H = 100$ Oe (squares), $H = 1000$ Oe (circles), $H = 10\,000$ Oe (triangles), and $H = 50\,000$ Oe (stars). Ferromagnetic state is stabilized and spans to lower-temperature region by enhancing of the external magnetic field $H$.

The $S$ of samples S1 and S2 changes its sign from positive to nearly constant negative value of $\sim 5\ \mu$V/K, while sample S3 keeps a positive sign with pronounced minimum at $T \sim 344$ K (see left inset of Fig. 2). This feature is reminiscent to metal-insulator transition and spin-state transition observed by other authors for $RBaCo_2O_{5+\delta}$ with doping close to $\delta = 0.50$.[9–12,18,19,33]

Temperature dependence of magnetization $M(T)$ is investigated for all samples in four intermediate magnetic fields up to 50 kOe ($H = 100$ Oe, 1 kOe, 10 kOe, and 50 kOe) and $T$

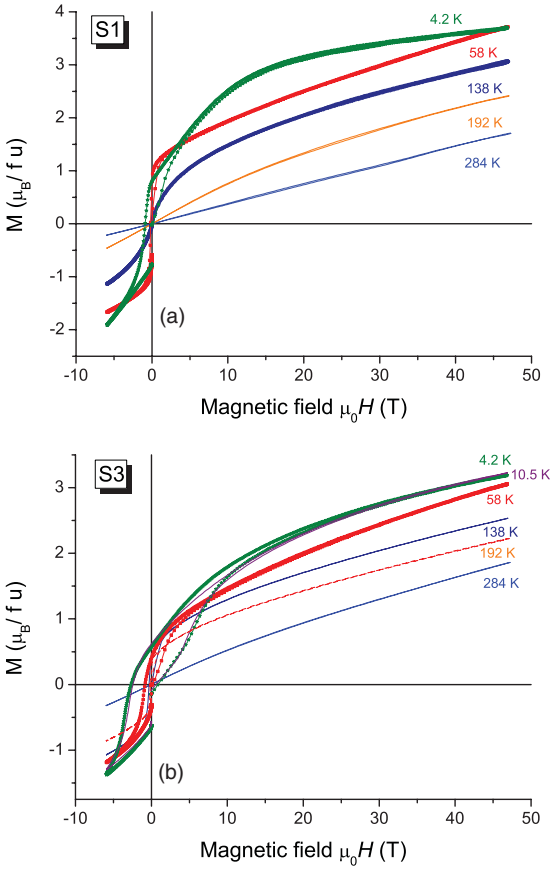


FIG. 4. (Color online) Magnetic-field dependence of the magnetization $M$ of samples (a) S1 and (b) S3. Measuring temperatures are indicated at the curves.

up to 300 K. The obtained results on polycrystalline samples $NdBaCo_2O_{5+\delta}$ are presented as magnetic susceptibility $M/H$ vs $T$ dependencies in Figs. 3(a), 3(b), and 3(c), for samples S1, S2, and S3, respectively.

We investigated also $M(T)$ correlation for sample S3 in a wider temperature range ($300\ \text{K} < T < 400$ K) and found well-pronounced change of the slope $dM/dT$ at $T \sim 343$ K (not shown). This feature is evidence for metal-insulator transition/spin-state-ordered transition of sample S3 and is reminiscent to those found by Taskin *et al.*,[10] Zhdanov *et al.*,[18] García-Fernández *et al.*,[19] and Frontera *et al.*[33] for $RBaCo_2O_{5.50}$ ($R$ = Gd and Pr) employing different characterization techniques. We can conclude that the sample $NdBaCo_2O_{5.52}$ behavior is very similar to that of a prototypical $RBaCo_2O_{5.50}$ composition.

Sample S1 ($\delta = 0.72$) behaves as a prototypical $GdBaCo_2O_{5.70}$ compound: ferromagnetic transition is shifted to lower temperatures $T < 150$ K, and the sample goes through successive paramagnetic metal (PMM)-paramagnetic insulator (PMI)-ferromagnetic insulator (FMI)-antiferromagnetic insulator (AFI) transitions during cooling in good agreement with proposed magnetic phase diagram (see Fig. 28 of Ref. 10). Sample S2 ($\delta = 0.55$) shows magnetic properties similar to the mix of behaviors of samples S1 and S3.

Below, we present $M(\mu_0 H)$ dependences in pulsed magnetic fields. Isothermal magnetization $M$ vs applied magnetic field $\mu_0 H$ ($-6\ \text{T} < \mu_0 H < 47$ T) dependencies of samples

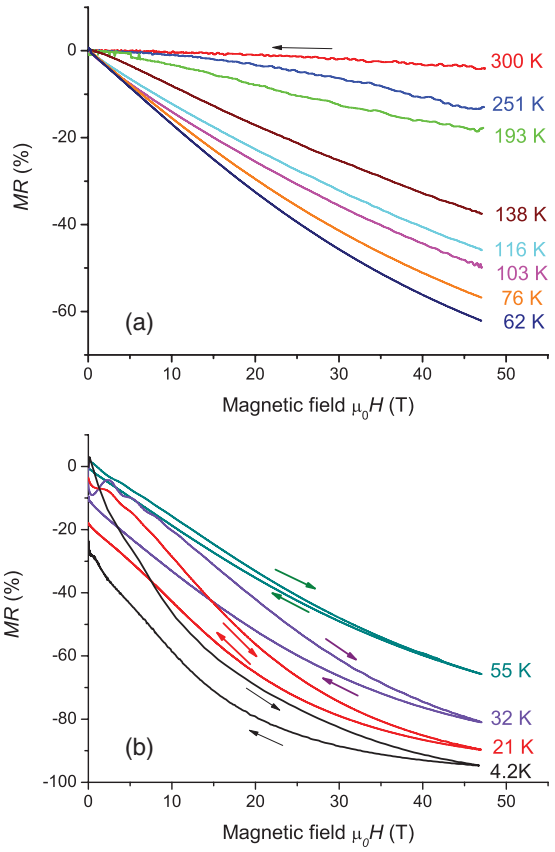


FIG. 5. (Color online) Magnetoresistance *MR* in dependence on magnetic field $\mu_0 H$ for sample S1 ($NdBaCo_2O_{5.72}$) measured in (a) the high-temperature range and (b) the low temperature range. The latter reveals hysteretic behavior. Here, branches for increasing and decreasing field are plotted.

S1 and S3 are recorded at five constant temperatures ($T$ = 284, 192, 135, 55, and 4.2 K) and shown in Figs. 4(a) and 4(b), respectively. Each curve was obtained after zero field cooling (ZFC) of the sample from room temperature (RT) to appropriate temperature and then recording $M$ in biasing pulsed magnetic field from zero up to 47 T, down to −6 T and finally from −6 T up to zero.

Sample S3 reveals similar behavior, but steep increase of $M$ is observed for runs at higher temperatures ($T$ = 192 K) than for the sample S1, in good agreement with the magnetic phase diagram for $GdBaCo_2O_{5.50}$ and significantly wider temperature range of FM phase ($T_C \sim 250$ K).[10] Sample S2 exhibits a mixed behavior (not shown) of those observed for samples S1 and S3.

Runs on sample S1 at $T$ = 284 and 192 K show linear paramagnetic dependences. Other runs reveal well-pronounced steep increase of $M(H)$ in low magnetic fields due to FM phase contribution of Co sublattice. Hysteretic behavior registered for runs at $T$ = 4.2 and 58 K is evidence for the first-order-field-induced AFM-FM transition. Such a behavior is in agreement with findings of Khalyavin *et al.*[17] for polycrystalline $NdBaCo_2O_{5.75}$ ($T_C \sim 150$ K) as well as with the magnetic phase diagram proposed in Ref. 10. One can notice that magnetization $M(T = 4.2$ K) starts to saturate in fields $\mu_0 H \sim 20$ T but still keeps increasing up to maximal magnetic field of 47 T.

Isothermal magnetization $M$ vs applied magnetic field $\mu_0 H$ ($-6$ T $< \mu_0 H <$ 47 T) dependencies of all samples were recorded at $T$ = 4.2 K (not shown). The coercive field of S3 ($\mu_0 H_c \sim 2.7$ T) is maximal but significantly smaller than that found for AFM-FM transition ($\mu_0 H_c \sim 15$ T) by Respaud *et al.*[4] for $GdBaCo_2O_{5.50}$.

We emphasize the systematic investigation of magnetoresistance of prototypical sample S1 ($NdBaCo_2O_{5.72}$) because of the lack of experimental data on correlation between charge transport and magnetic ordering up to now. To the best of our knowledge, there are only two works on magnetotransport in high-magnetic fields but on prototypical $RBaCo_2O_{5.50}$ compound: Respaud *et al.*[4] have investigated polycrystalline $GdBaCo_2O_{5.50}$ and determined $\mu_0 H$–$T$ phase diagram in pulsed magnetic fields up to 35 T; while magnetic and magnetotransport behavior of single crystal $EuBaCo_2O_{5.50}$ has been acquired in dc magnetic fields up to 33 T by Zhou *et al.*[21]

The magnetoresistance results $MR = [R(0) - R(H)]/R(0)$ vs $\mu_0 H$ of a sample S1 ($\delta$ = 0.72) show no hysteresis in the high-temperature range, $T$ = 60–300 K [see Fig. 5(a)]. In the low-temperature range, $T$ = 4.2–55 K, there is a significant hysteresis between increasing and decreasing parts of the magnetic field pulse. The observed hysteretic behavior of *MR* at temperatures $T <$ 55 K [Fig. 5(b)] could be ascribed to first-order AFM-FM phase transition, like found by Respaud *et al.*[4]

## IV. DISCUSSION

Above the temperature of about 130 K, conductivity of all investigated samples deviates from exponential expression (see Fig. 1). The shape of $\rho(T)$ between 130 and 300 K is concave for samples S1 and S2 in contrast to the convex ones in the case of S3 sample. Below 130 K down to about 4, 3, and 20 K, the resistivity increases for the samples S3, S2, and S1, respectively. It is the range where conductivity changes exponentially. At low temperatures, i.e. below 4 and 20 K for samples S3 and S1, respectively, the resistivity starts to saturate.

At low temperatures, the conductivity $\sigma(T) = 1/\rho(T)$ can be roughly described by the expression (see dashed lines in the inset of Fig. 1):[40]

$$1/\rho_{LT} = A_0 \exp\left[-\left(\frac{T_0}{T}\right)^{1/4}\right], \quad (1)$$

where the exponential term denotes variable range hopping and $T_0$ is the characteristic temperature defined by:

$$T_0 = \frac{18}{k_B N_0(E_F)\xi^3}, \quad (2)$$

where $k_B$ is the Boltzmann constant, $N_0(E_F)$ is the electronic density of states at the Fermi level and in the absence of electron-electron interaction, while $\xi$ is the localization length of the relevant electronic wave function. Parameters $A_0$ and $T_0$ are collected in Table I.

Below about 130 K, the $1/\rho(T)$ data for all samples do not follow an Arrhenius equation, which would be appropriate for a simple single-gap semiconductor. Instead, these data are

TABLE I. The fitting parameters of Eqs. (1) and (3).

| Sample | $A_0(\Omega\cdot\text{cm})^{-1}$ | $T_0/k_B$(K) | $A_1(\Omega\cdot\text{cm})^{-1}$ | $\Delta_1/k_B$(K) | $A_2(\Omega\cdot\text{cm})^{-1}$ | $\Delta_2/k_B$(K) |
|---|---|---|---|---|---|---|
| S1 | 162500 | 29.0 | 498.3 | 382 | 44930 | 997 |
| S2 | 128176 | 31.1 | 685.3 | 334 | 67747 | 997 |
| S3 | 167174 | 35.6 | 206.5 | 332 | 10715 | 997 |

described by a two-gap expression completed by the term of variable range hopping [see Eq. (3), the solid lines in Fig. 1, and fitting parameters shown in Table I]:[41–43]

$$1/\rho = A_0 \exp\left[-\left(\frac{T_0}{T}\right)^{1/4}\right] + A_1 \exp\left(-\Delta_1/T\right) + A_2 \exp\left(-\Delta_2/T\right), \quad (3)$$

where the parameters $A_i$ and the activation energies $\Delta_i/k_B$ are collected in Table I. A possible interpretation of these fits is that the large gap $\Delta_2$ describes the intrinsic energy gap for $NdBaCo_2O_{5+\delta}$, whereas $\Delta_1$ describes the doped/impurity acceptor/donor states in the gap. In order to show the trend of activation energies with the hole doping, we have kept the larger activation energy $\Delta_2/k_B$ constant, taking arbitrarily an average value for three samples (=997 K). It allows obtaining the monotonic dependence of the $\Delta_1/k_B$ in relation to the hole doping. Thus, $\Delta_1/k_B$ = 382, 334, and 332 K for the samples with $\delta$ = 0.72, 0.55, and 0.52, respectively, which shows the trend in these values with the hole doping. Both the plot log $\rho$ vs $T^{1/4}$ and the data fit by Eq. (1) indicate that the electrical transport at low temperatures ($T$ = 3–9 K for samples S3 and S2) should occur by hopping of charge carriers, probably between localized 4*f* states of neodymium Nd or/and localized states of impurities. The characteristic temperature $T_0$ for the all samples varies from about 29 to 36 K (Table I). In extrinsic regime, i.e. below 3 K for sample S3 and 20 K for sample S1, the impurities states dominate the transport results on conductivity saturation.[44]

Above 10 K (for samples S3 and S2) and above $T \sim$ 30 K (for sample S1) up to 130 K, the activation processes mainly contribute. Assuming the process when an electron comes from the valence to conduction band in the valence band, there is a second charge carrier, the hole. Thus, the activation energies $E_{g2}$ = 172 meV ($E_g = 2\Delta$), whereas $E_{g1}$ is equal to 66, 58, and 57 meV for samples S1, S2, and S3, respectively. Such a two-gaps scenario for conductivity should be justified if one will look for the calculated density of states for various impurity concentrations presented in Ref. 45.

At higher temperatures, i.e. above 130 K, electron-phonon interaction should be taken into account with a weakening activation process at the same time. Above $T_2^*$ = 250 K the concentration of charge carriers increases approximately exponentially, and the resistivity for samples S1 and S2 starts to saturate, while for S3, it has an unexpected convex shape due to the metal-insulator transition at $T_{MI} \sim$ 344 K (see Fig. 1).

We further analyze the differences between available experimental data on conductivity of single crystals and polycrystalline $RBaCo_2O_{5+\delta}$ samples in order to distinguish between intra- and intergrain contributions as well as on different hopping modes. Indeed three modes of hopping have been found in $GdBaCo_2O_{5+\delta}$ single crystals (see Ref. 10) depending on oxygen stoichiometry: (1) activated behavior for prototypical compound with $\delta$ = 0.50 (in good agreement with data of Zhou *et al.*[21] on single crystal $EuBaCo_2O_{5+\delta}$); (2) VRH for the zone close to $\delta$ = 0.50 with either electron or hole doping ($0.45 < \delta < 0.525$); and (3) Efros–Shklovskii behavior for electron-doped cobaltites ($0.165 < \delta < 0.44$) (see Fig. 8 of Ref. 10).

We try to fit our experimental data for all three samples employing above-mentioned hopping models and found best approximations for the VRH mode and activation behavior. The details of fitting procedures as well as temperature regions of their validity are presented in Table II. The goodness of the fits made for $\rho(T)$ curves is represented by the coefficient of determination, $R^2 \equiv 1 - \frac{SS_{\text{err}}}{SS_{\text{tot}}}$, where $SS_{\text{err}} = \sum_i (y_i - f_i)^2$ is the residual sum of squares and $SS_{\text{tot}} = \sum_i (y_i - \overline{y})^2$ is the total sum of squares (proportional to the sample variance). From the values of $R^2$, one can see that the best fit was obtained in the case of sample S1 within the temperature region of 29–231 K.

Sample S3: One can notice good accordance between location of activation behavior fit zone (114–266 K) of our

TABLE II. The fitting procedures used to approximate $\rho(T)$ dependences of samples S1, S2, and S3, their temperature regions of validity, linear fit parameters, $A$, $B$, and the coefficient of determination $R^2$.

| Sample | Correlation | Temperature region | $A$ ($\Omega\cdot$cm) | $B$ ($\Omega\cdot$cm K$^{-1}$) | $R^2$ |
|---|---|---|---|---|---|
| S1 | Activation behavior | 114–265 K | −7.8 | 461.0 | 0.99919 |
| S1 | VRH | 29–231 K | −6.9 | 17.2 | 0.99958 |
| S1 | VRH | 1.9–9.5 K | −0.8 | 4.6 | 0.99546 |
| S2 | Activation behavior | 121–251K | −9.4 | 612.8 | 0.99919 |
| S2 | VRH | 39–120 K | −7.7 | 19.6 | 0.99933 |
| S2 | VRH | 3–39 K | −5.5 | 14.2 | 0.999560 |
| S3 | Activation behavior | 114–266 K (AFM1 zone $T_{N1} <$ 265 K); Zone III (AFM/FM/INS) 270–170 K | −6.0 | 363.7 | 0.99914 |
| S3 | VRH | 32–129 K AFM2 zone, $T_{N2} <$ 160 K;[15] Zone IV (AFM/INS) $T <$ 170 K.[19] | −7.7 | 21.3 | 0.9993 |
| S3 | VRH | 3–31 K | −5.1 | 152 487 | 0.99955 |

polycrystalline sample $NdBaCo_2O_{5.52}$ with the magnetic phase diagram for polycrystalline sample $NdBaCo_2O_{5.50}$ proposed by Jarry *et al.*,[16] (especially for AFM1 phase zone below $T <$ 265 K). This temperature zone also partially coincides with zone III proposed by Garcia-Fernandes *et al.*[19] (AFM/FM insulators; 170–270 K).

Sample S1: VRH fit (29–231 K) and activation behavior fit (114–265 K) give nearly the same accuracy but former spans on wider temperature zone. It is important to note that this wide VRH fit zone includes three different magnetic phase zones, namely, PMM phase down to 135 K, ferromagnetic metal (FMM) phase (85 K $< T <$ 135 K), and AFI3 phase (4 K $< T <$ 85 K) after the proposed magnetic phase diagram of $GdBaCo_2O_{5+\delta}$ ($\delta \sim 0.75$) (see Fig. 28 of Ref. 10). We can conclude that charge transport for sample S1 is determined mainly by VRH in good accordance with observed SSO and phase separation at nanoscale by Jarry *et al.*[16] on polycrystalline sample $NdBaCo_2O_{5.50}$.

Sample S2: Activation behavior fit (121–251 K) and two VRH fits at lower temperatures (39–120 and 3–39 K) give nearly the same accuracy in three successive temperature zones. It is important to note that the first activation fit zone includes PMM phase after Ref. 10, while VRH zones coincide roughly with FMM phase (85–135 K) and AFI3 phase (4–85 K).

Let us discus the thermoelectric power behavior (Fig. 2). The derivatives $dS/dT$ vs log $T$ from 50 K up to 350 K for two samples S1 and S2 are presented in the right inset of Fig. 2. The crossover of two straight lines passing through a group of points determines the characteristic temperatures ($T_1{}^*$ and $T_2{}^*$), which split temperature range on parts where the different mechanisms of conductivity are dominant.[46,47] The temperature dependencies of thermoelectric power $S(T)$ for samples S1 and S2 are qualitatively similar; below 350 K down to about 250 K $S(T)$, it is negative and slightly increases then changes a sign at 243 K and 220 K for samples S2 and S1, respectively. Next, the $S$ accelerates increase with decreasing $T$ down to the characteristic temperature $T_1{}^* = 130$ K at the same time a slope is higher for sample S2. Below $T_1{}^*$ is observed a drop of velocity of increasing $S$ values. The $S(T)$ dependence for sample S3 is quite different from that of samples S1 and S2. It is positive in the entire measured range. Below 350 K, it passes through a minimum ($S_{\min} \approx 0\ \mu V{\cdot}K^{-1}$) at about 344 K and next increases with a high slope when $T$ decreases. A high maximum of about 164 $\mu V{\cdot}K^{-1}$ is achieved at $T_{\max} = 108$ K. The main difference in $S(T)$ dependence for S3 sample in comparison to S1 and S2 ones is convex shape of the former. Also, the characteristic temperatures $T_1{}^*$ and $T_2{}^*$ are shifted to the values of 250 and 335 K, respectively.

The thermoelectric power of semiconductors should fulfill a relation:[48]

$$S = \frac{k_B}{e}\left[\left(\frac{5}{2} + q\right) - \frac{E_F}{k_B T}\right], \tag{4}$$

where $E_F$ is the Fermi energy, and $q$ is the exponent in the dependence of relaxation time as a function of energy: $\tau = \tau_0 E^q$, for example, for scattering on acoustic oscillations $q = -1/2$, while for scattering on ionized admixtures $q = 3/2$.

The solids lines in Fig. 2 represent the data fit to Eq. (4): $S(T) = a - b/T$ , where the parameters $a$ and $b$ are equal to $-15.85\ \mu V{\cdot}K^{-1}$ and $-4{,}148.9\ \mu V{\cdot}K^{-2}$ or $-65.72\ \mu V{\cdot}K^{-1}$ and $-15\,245.1\ \mu V{\cdot}K^{-2}$ for samples S1 and S2, respectively. The thermoelectric power for samples S2 above 123 K up to 180 K fulfilled the Eq. (4) used for semiconductors. In the case of sample S1, the upper boundary of this temperature range is considerably limited. Near $T_2{}^*$, the $S$ for S1 and S2 changes sign to negative and slightly decreases with increasing temperature. It is a spontaneous region in semiconductors where concentrations of electrons and holes are similar. The thermoelectric powers of electrons $S_n$ and holes $S_p$ are comparable and have an opposite sign. Here, $S_n$ dominates due to the higher mobility of electrons. It is obvious that, for sample S3, the holes contribution is dominant, and the convex shape of $S(T)$ dependence results from the MI transition. At low-$T$ where the Mott variable range hopping dominates, the $S$ should vary as $T^{1/2}$ (Refs. 49 and 50), but due to too-high resistivity of samples S2 and S3, the $S$ was not measured in this range. The dashed line in Fig. 2 presents a hypothetical thermal dependence of $S \sim T^{1/2}$ at low $T$ for the S2 sample.

It is worth noticing that temperatures $T_1{}^* = 130$ and 250 K for samples (S1 and S2) and S3, respectively, are consistent with temperatures of magnetic transitions observed in $\chi = M/H(T)$ dependencies of Fig. 3 as well as $T_2{}^* = 335$ K of sample S3 indicates the onset of the MI transition found by additional $M(T)$ measurements at $T \sim 343$ K (not shown).

It is seen that thermoelectric power of $NdBaCo_2O_{5+\delta}$ could not be explained employing a semiconductor approach only. Comprehensive investigation of thermoelectric power $S$ of $GdBaCo_2O_{5+\delta}$ and $NdBaCo_2O_{5+\delta}$ single crystals have been carried out by Taskin *et al.*[10,12] These authors have succeeded in explaining striking large values of thermoelectric power $S$ as well as its remarkable divergence near $\delta = 0.50$ ($S$ varies from 800 $\mu V{\cdot}K^{-1}$ to $-700\ \mu V{\cdot}K^{-1}$) by estimation of entropy contribution of charge carriers (electrons by $Co^{2+}$ ions, holes by $Co^{4+}$ ions, or host $Co^{3+}$ ions). After Ref. 12, both strong electron correlations and spin-orbital degeneracy are responsible for experimentally registered large thermoelectric power in transition-metal oxides $RBaCo_2O_{5+\delta}$ ($R$ = Gd and Nd). It was found that $GdBaCo_2O_{5+\delta}$ and $NdBaCo_2O_{5+\delta}$ compounds possess virtually the same temperature and doping correlation as well as even very close (nearly the same) experimental values of $S$ [see Figs. 3(a) and 3(b) of Ref. 12 and resistivity $\rho$ [see Figs. 2(a) and 2(b) of Ref. 12.

We used our experimental data of thermoelectric power $S$ to estimate oxygen stoichiometry of sample S3 [$S_{\max}(T = 108\ K) = 164\ \mu V{\cdot}K^{-1}$] and found $0.519 < \delta(S3) < 0.590$ [Fig. 3(b) in Ref. 11] or $0.515 < \delta(S3) < 0.552$ (Fig. 10 of Ref. 10). These estimation ranges are in agreement with the tuned-by-annealing procedure (discussed earlier in the experimental section) value of oxygen doping, namely $\delta(S3) = 0.52$.

It could be useful to study magnetotransport in layered cobaltites by yet employed approaches on other magnetic oxides like cuprates, manganites, ruthenates, etc. We have preliminary experience on studying polycrystalline and epitaxially grown manganite thin films of $La_{0.7}Ca_{0.3}MnO_3$ and $La_{0.7}Sr_{0.3}MnO_3$ grown by magnetron sputtering (MS) or pulsed laser deposition (PLD) techniques on different substrates.[51–59] It is well established that, in manganites, the double-exchange (DE) mechanism competes with charge and orbital ordering. The spin-tunneling magnetoresistance taking

place in low magnetic fields at grain boundaries (GBs) in polycrystalline manganite samples (due to good spin polarization of individual manganite grains at low temperatures) vanishes at higher temperatures.[60–64] It is known that GBs possess a strongly enhanced electrical resistance. In polycrystalline thin $La_{0.7}Ca_{0.3}MnO_3$ and $La_{0.7}Sr_{0.3}MnO_3$ films or ceramics, the intergrain resistance contribution dominates the measured electrical resistance (in particular at temperatures far below the ferromagnetic Curie temperature $T_C$). At the coercive field, the magnetization of the polycrystalline material is zero, and the magnetizations of the grains are randomly oriented. This leads to a higher resistance state compared to the low-resistance state achieved above the saturation field, when all the magnetizations of grains are parallel. Surprisingly, *MR* in manganites does not saturate at the bulk saturation field. After Kozlova *et al.*[65] in the case of polycrystalline $La_{0.7}Sr_{0.3}MnO_3$ manganite, the high-field (above 1 T and up to 50 T) magnetoconductance increases linearly with the magnetic field at temperatures up to $T < 100$ K and does not show any saturation. These results have been explained (see Ref. 65) within a model of second-order tunneling through GBs proposed by Lee *et al.*,[61] and strong AFM coupling at the grain boundaries has been deduced.

In sharp contrast with the behavior observed in manganites, double perovskites $Sr_2FeMoO_6$ show a tendency to saturation in high magnetic fields.[66] The *MR* behavior of double perovskite $(Ba_{0.8}Sr_{0.2})_2FeMoO_6$ has been explained within a model for intergrain magnetoresistance in which the GBs magnetic state is possibly spin glass.[67] It has been found that the magnetoconductance ($G$) of double perovskites follows the functional form $G \sim \exp[-(H_0/H)^{1/2}]$ up to $B = 5$ T for $Sr_2FeMoO_6$ (Ref. 66) and up to 50 T for $(Ba_{0.8}Sr_{0.2})_2FeMoO_6$ (Ref. 67).

Although both $La_{0.7}Ca_{0.3}MnO_3$ manganites and hole-doped cobaltites $RBaCo_2O_{5+\delta}$ reveal huge negative *MR* at low temperatures, its origin seems to be different. The double-exchange (DE) mechanism and high conductance of the ferromagnetic metal phase, taking place in manganites, are not relevant for cobaltites. Taskin *et al.*[11] proposed a new scheme, a kind of magnetic-field-effect transistor where the charge carrier injection into a 2D semiconducting channel is controlled by a magnetic state of neighboring ligands. After Taskin *et al.*,[10,11] ordering of adjacent FM ladders in external magnetic field (applied along the *ab* plane) resulted in significant reduction of the insulating gap size, steplike increase of the number of carriers, and strong decrease of resistivity $\Delta\rho_c/\rho_c$. It has been shown (see Fig. 25 of Ref. 10) that activation energy is actually diminished by the magnetic field, and thus the *MR* grows by decreasing temperature. Simple activation fits $\rho_c \sim \exp(\Delta/T)$ for both the AFM and FM states have been found for single-crystal $GdBaCo_2O_{5.50}$ in zero- and high-magnetic field, respectively. We tried to use the same fit to our experimental data but failed. Instead, VRH fit gives good approximation in the temperature region 41 K $< T <$ 193 K (see Fig. 6).

This is in agreement with results found by Respaud *et al.*[4] for polycrystalline $GdBaCo_2O_{5.50}$ samples (VRH fit). We estimate the relation $\xi(B = 47\ \text{T})/\xi\ (B = 0) \sim 1.4$ for $NdBaCo_2O_{5.72}$. The obtained value differs by one order of magnitude in comparison with that found in Ref. 4 [$\xi(B = 35$ T$)/\xi(B = 0) \sim 12$]. The reason for this could be ascribed to possible different GBs thickness (extrinsic parameter determined by growth and annealing processes) or different GBs magnetic state (intrinsic parameter determined by magnetic phase diagram of either compound). Another magnetoconductance behavior dissimilarity comparing $NdBaCo_2O_{5.72}$ with $RBaCo_2O_{5.50}$ ($R$ = Gd and Eu) is the lack of step before steep *MR* increase in lowest temperatures, especially at $T =$ 4 K. Differences found in magnetoconductance behavior of two prototypical phases $\delta = 0.5$ and 0.75 could be ascribed to different magnetic phase diagrams found and a possible different type of anisotropy. Indeed, in this temperature region, a $NdBaCo_2O_{5.75}$ sample exhibits ferrimagnetic state after Ref. 17 (Co sublattice and Nd sublattice) instead of AFI for $GdBaCo_2O_{5.50}$ after Ref. 10.

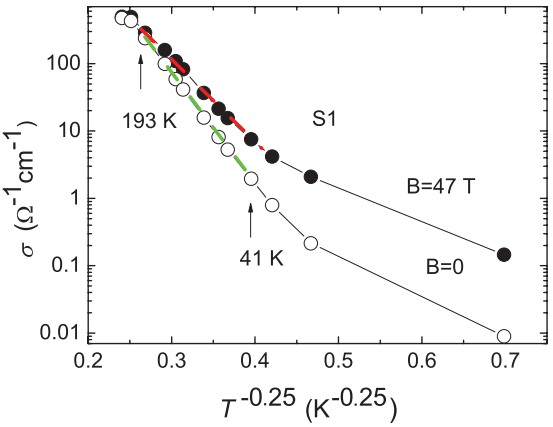


FIG. 6. (Color online) Electrical conductivity $\sigma$ vs $T^{-0.25}$ for sample S1 ($NdBaCo_2O_{5.72}$) measured in zero-magnetic field and $B =$ 47 T. The dashed lines display VRH fits at region 41 K $< T <$ 193 K.

Let us estimate also the influence of possible oxygen distribution gradient on *MR*. There is an indication of the presence of small oxygen gradient in sample S1 due to not enough sharp quench after 24 hours holding at 250 °C (see Lobanovskii *et al.*[7]): FM/AFM transition is more smooth and spread in temperature [see Fig. 3(a)] instead of a sharp one for single-crystal $GdBaCo_2O_{5.70}$ [see Fig. 18(c) of Ref. 10. The percolation through grains with close values of resistivity in the region of heavy hole doping ($\delta \sim 0.75$) has not changed *MR* behavior drastically (but it would be critical for the zone $\delta \sim 0.50$).[10,22] One can suppose a crucial influence on *MR* comes from phase separation phenomena and especially by specific SSO mechanism taking place in $RBaCo_2O_{5.50}$.[15,16] The percolation through many tiny (nano)phase separated SSO clusters has to become determinant for *MR* behavior.

Further, we analyze isothermal magnetoconductance of the sample $NdBaCo_2O_{5.72}$ and succeed to fit it by $G(H,T)/G(0) = G_0\exp(H/H_0)$ dependence (see Fig. 7 and Table III).

The obtained correlation is not known so far. It differs with simple linear dependence found on polycrystalline manganites $La_{0.7}Sr_{0.3}MnO_3$.[65] The reason should be the specific origin of the AFM-FM transition in cobaltites. As stated in Ref. 10, observed AFM-FM switching of $GdBaCo_2O_{5.50}$ in a magnetic field is a metamagnetic transition. It takes place within the ordered spin state and is governed by the relative reorientation of weakly coupled spin sublattices. We consider the physical

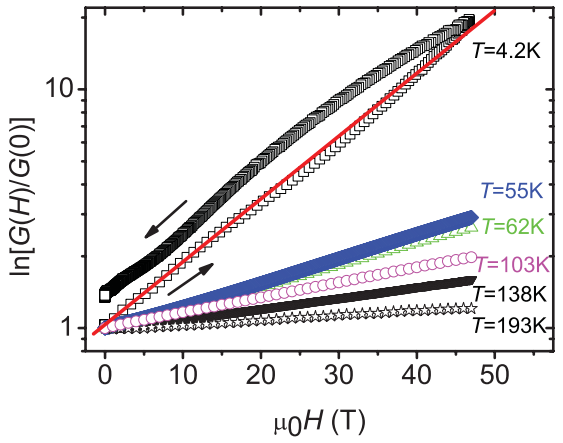


FIG. 7. (Color online) Electrical conductance $G(H)/G(0)$ vs $\mu_0 H$ dependence for sample S1 of $NdBaCo_2O_{5.72}$ measured at variable temperatures 4.2 K $< T <$ 193 K (as marked in figure). The zone 55 K $< T <$ 138 K coincides with the FM region after Ref. 17. The solid line displays the fit to $G(H, T_{const})/G(0) = G_0 \exp(H/H_0)$ dependence for run-up at $T = 4.2$ K (fits details shown in Table III).

meaning of the parameter $H_0$ as the magnetic field value in which spin sublattices' reorientation is completed and *MR* value saturated. One can notice how strongly this field of full spin sublattices' reorientation is influenced by the temperature (see Table III): from $H_0 = 16$ T at $T = 4.2$ K up to $H_0 = 217.4$ T at $T = 193$ K. The obtained value $H_0 = 16$ T ($T = 4.2$ K) is consistent with $M(\mu_0 H)$ and $MR(\mu_0 H)$ dependences [Figs. 4(a) and 5(b)]. Such estimation of $H_0$ is not found up to now and is our own contribution to charge transport of hole doped $NdBaCo_2O_{5+\delta}$ system ($0.52 < \delta < 0.72$) in wide magnetic field region. It becomes possible due to investigations in pulsed magnetic fields up to 47 T.

Another pro argument is the apparent discrepancy found between noticeably smaller FM moments of polycrystalline $GdBaCo_2O_{5.50}$ samples (about 0.3 $\mu_B$/f. u. at $T = 0$ K after Ref. 1) and that of detwinned single crystals $GdBaCo_2O_{5.50}$ ($\sim$0.8 $\mu_B$/Co after Fig. 24 of Ref. 10). The discrepancy of magnetic moments implies that the Ising spin anisotropy makes magnetic moments in the *b* and *c* axes oriented crystallites to remain nearly invisible in polycrystalline samples. This feature has been found to be nearly independent by oxygen stoichiometry (see Taskin *et al.*[10]), and so we can deduce that the magnetoconductance in hole-doped polycrystalline $NdBaCo_2O_{5.72}$ is realized mainly through the *a*-oriented grains

TABLE III. Fit data to isothermal magnetoconductance $G(H, T)/G(0) = G_0 \exp(H/H_0)$, run temperature, $T$ [K], fit constants $G_0$, $H_0$ [T], and the coefficient of determination $R^2$.

| Run temperature $T$, [K] | $G_0$ | $H_0$, [T] | $R^2$ |
|---|---|---|---|
| 4.2 K run-up | 0.98 | 16.0 | 0.99872 |
| 55 K run-up | 1.03 | 43.5 | 0.99896 |
| 62 K | 0.98 | 47.5 | 0.99979 |
| 103 K | 1.01 | 69.0 | 0.99997 |
| 138 K | 0.98 | 97.3 | 0.99976 |
| 193 K | 0.98 | 217.4 | 0.99597 |

due to the strong decrease of resistivity $\Delta\rho_c/\rho_c$ in the external magnetic field along *a* axis.

It is worth noticing that $G(H, T)/G(0) = G_0 \exp(H/H_0)$ dependence holds very well (see Table III, $R^2 > 0.9989$) in the temperature region where FM state appears, coexists with AFM state, and AFM-FM switching takes place.[17] This dependence could be extended to the run-up process at $T =$ 4.2 K (see Fig. 7 and Table III), where the fit remains good, too. For the hysteretic run-down process, however, the fit is deteriorated. Here, *MR* of S1 in the lowest *T* zone [Fig. 5(b)] reveals complicated hysteretic behavior, which could be ascribed to the ferrimagnetic state in this zone ($T < 40$ K).[17]

As mentioned above, the SSO and phase separation at nanoscale have been experimentally proved by Luetkens *et al.*[15] and Jarry *et al.*[16] Depending on the rare earth element, they have deduced two types of SSO (A1 and A2) in the AFM1 phase and up to four different types of SSO (A1–A4) in the AFM2 phase. One can suppose that multiple temperature zones registered by us with different VRH or activation behavior modes (see details in Tables II and III) could be ascribed to modified SSO. The spin state ordering could be developed by changing temperature and external magnetic field and especially by AFM-FM transition.

## V. CONCLUSIONS

Magnetic and transport properties of the $NdBaCo_2O_{5+\delta}$ system were studied in a less-investigated hole-doped region ($0.52 < \delta < 0.72$) and in pulsed magnetic fields up to 47 T. Below $T < 130$ K, the conductance in zero-magnetic field is described by a two-gap expression completed by the term of variable range hopping. The thermoelectric power $S(T)$ measurements confirm the magnetic phase diagram found by magnetic and electric transport investigations. It is shown that FM behavior of $NdBaCo_2O_{5+\delta}$ ($0.52 < \delta < 0.72$) is stabilized and spans in lower temperatures by increasing external magnetic field in agreement with structural and magnetic phase diagrams found on $NdBaCo_2O_{5.75}$,[17] $NdBaCo_2O_{5.50}$,[16] and $GdBaCo_2O_{5+\delta}$ systems.[10] The VRH mode gives good approximation in zero- and high-magnetic field 47 T. The isothermal magnetoconductance of $NdBaCo_2O_{5.72}$ is well fitted by $G(H, T)/G(0) = G_0 \exp(H/H_0)$ dependence at the temperature region 55 K $< T <$ 138 K (the zone where FM state appears).[17] The parameter $H_0$ is considered as the magnetic field of full spin sublattices' reorientation and *MR* saturation. The magnetoconductance in $NdBaCo_2O_{5.72}$ is possibly realized through the *a*-oriented grains (strong decrease of resistivity $\Delta\rho_c/\rho_c$ in magnetic field along the *a* axis). The deduced reason for observed magnetoconductance behavior is the specific origin of the AFM-FM transition in layered cobaltites. It is assumed to be a metamagnetic transition governed by the relative reorientation of weakly coupled spin sublattices in good accordance with spin-state ordering and phase separation proved experimentally.[10,11,15,16]

## ACKNOWLEDGMENTS

Part of this work has been supported by EuroMagNET under the EU contract RII3-CT-2004-506239 of the 6th Framework "Structuring the European Research Area, Research Infra-structures Action."

*Present address: Dr. Emil Vlakhov, Georgi Nadjakov Institute of Solid State Physics, Bulgarian Academy of Sciences, 72 Tzarigradsko Chaussee Blvd, 1784 Sofia, Bulgaria; emil_vlakhov@abv.bg

[1] I. O. Troyanchuk, N. V. Kasper, D. D. Khalyavin, H. Szymczak, R. Szymczakm, and M. Baran, Phys. Rev. B **58**, 2418 (1998); Phys. Rev. Lett. **80**, 3380 (1998).

[2] A. Maignan, C. Martin, D. Pelloquin, N. Nguyen, and B. Raveau, J. Solid State Chem. **142**, 247 (1999).

[3] V. Pralong, V. Caignaert, S. Hebert, A. Maignan, and B. Raveau, Solid State Ionics **177**, 1879 (2006).

[4] M. Respaud, C. Frontera, J. L. Garcia-Munoz, M. A. G. Aranda, B. Raquet, J. M. Broto, H. Rakoto, M. Goiran, A. Llobet, and J. R. Rodriges-Carvajal, Phys. Rev. B **64**, 214401 (2001).

[5] M. Baran, V. I. Gatalskaya, R. Szymczak, S. V. Shiryaev, S. N. Barilo, K. Piotrowski, G. L. Bychkov, and H. Szymczak, J. Phys. Condens. Matter **15**, 8853 (2003).

[6] F. Fauth, E. Suard, V. Caignaert, and I. Mirebeau, Phys. Rev. B **66**, 184421 (2002).

[7] L. S. Lobanovskii and I. O. Troyanchuk, JETP Lett. **82**, 719 (2005).

[8] L. S. Lobanovskii, I. O. Troyanchuk, H. Szymczak, and O. Prokhnenko, J. Exp. Theor. Phys. **103**, 740 (2006).

[9] S. Roy, I. S. Dubenko, M. Khan, E. M. Condon, J. Craig, and N. Ali, Phys. Rev. B **71**, 024419 (2005).

[10] A. A. Taskin, A. N. Lavrov, and Yoichi Ando, Phys. Rev. B **71**, 134414 (2005).

[11] A. A. Taskin, A. N. Lavrov, and Yoichi Ando, Phys. Rev. Lett. **90**, 227201 (2003).

[12] A. A. Taskin, A. N. Lavrov, and Yoichi Ando, Phys. Rev. B **73**, 121101 (2006).

[13] S. Sugano, Y. Tanabe, and H. Kamimura, *Multiplets of Transition-Metal Ions in Crystals* (Academic, New York, 1970).

[14] M. Imada, A. Fujimori, and Y. Tokura, Rev. Mod. Phys. **70**, 1039 (1998).

[15] H. Luetkens, M. Stingaciu, Yu. G. Pashkevich, K. Conder, E. Pomjakushina, A. A. Gusev, K. V. Lamonova, P. Lemmens, and H.-H. Klauss, Phys. Rev. Lett. **101**, 017601 (2008).

[16] A. Jarry, H. Luetkens, Y. G. Pashkevich, M. Stingaciu, E. Pomjakushina, K. Conder, P. Lemmens, and H. H. Klaus, Physica B doi: 10.1016/j.Physb.2008.11.178 (2009).

[17] D. D. Khalyavin, O. Prokhnenko, N. Stüßer, V. Sikolenko, V. Efimov, A. N. Salak, A. A. Yaremchenko, and V. V. Kharton, Phys. Rev. B **77**, 174417 (2008).

[18] K. R. Zhdanov, M. Yu. Kameneva, L. P. Kozeeva, and A. N. Lavrov. Phys. Solid State **52**, 1688 (2010).

[19] M. García-Fernández, V. Scagnoli, U. Staub, A. M. Mulders, M. Janousch, Y. Bodenthin, D. Meister, B. D. Patterson, A. Mirone, Y. Tanaka, T. Nakamura, S. Grenier, Y. Huang, and K. Conder, Phys. Rev. B **78**, 054424 (2008).

[20] D. Chernyshov, V. Dmitriev, E. Pomjakushkina, K. Conder, M. Stingaciu, V. Pomjakushkin, A. Podlesnyak, A. A. Taskin, and Y. Ando, Phys. Rev. B **78**, 024105 (2008).

[21] Z. X. Zhou and P. Schlottmann, Phys. Rev. B **71**, 174401 (2005).

[22] S. Streule, A. Podlesnyak, D. Sheptyakov, E. Pomjakushina, M. Stingaciu, K. Conder, M. Medarde, M. V. Patrakeev, I. A. Leonidov, V. L. Kozhevnikov, and J. Mesot, Phys. Rev. B **73**, 094203 (2006); S. Streule, A. Podlesnyak, J. Mesot, M. Medarde, K. Conder, E. Pomjakushina, E. Mitberg, and V. Kozhevnikov, J. Phys. Condens. Matter **17**, 3317 (2005).

[23] A. Tarancón, D. Marrero-López, J. Peña-Martínez, J.C. Ruiz-Morales, and P. Núñez, Solid State Ionics **179**, 611 (2008).

[24] H. Gu, H. Chen, L. Gao, Y. Zheng, X. Zhu, and L. Guo, Int. J. of Hydrogen Energy **34**, 2416 (2009).

[25] F. Wang, Q. Zhou, T. He, G. Li, and H. Ding, J. Power Sources **195**, 3772 (2010).

[26] V. G. Prokhorov, Y. P. Lee, K. W. Kim, V. M. Ishchuk, and I. N. Chukanova, Phys. Rev. B **66**, 132410 (2002).

[27] D. Fuchs, T. Schwarz, O. Moran, P. Schweiss, and R. Schneider, Phys. Rev. B **71**, 092406 (2005).

[28] A. D. Rata, A. Herklotz, K. Nenkov, L. Schultz, and K. Dörr, Phys. Rev. Lett. **100**, 076401 (2008).

[29] M. A. Torija, M. Sharma, M. R. Fitzsimmons, M. Varela, and C. Leighton, J. Appl. Phys. **104**, 023901 (2008).

[30] E. Vlakhov, R. Szymczak, M. Baran, K. Piotrowski, A. Szewczyk, W. Paszkowicz, L. Lobanovski, S. Matyasik, K. Nenkov, and H. Szymczak, Acta Physika Polonica A **115**, 89 (2009).

[31] E. Vlakhov, L. Neshkov, T. Nurgaliev, E. Mateev, Y. Marinov, L. Lakov, and K. Toncheva, Nanoscience & Nanotechnology **8**, 141 (2008); E. Vlakhov, K. Nenkov, L. Neshkov, B. Blagoev, E. Mateev, and T. Nurgaliev, *ibid.* **10**, 211 (2010).

[32] J. C. Burley, J. F. Mitchell, S. Short, D. Miller, and Y. Tang, J. Solid State Chem. **170**, 339 (2003).

[33] C. Frontera, J. L. García-Muñoz, A. E. Carrillo, M. A. G. Aranda, I. Margiolaki, and A. Caneiro, Phys. Rev. B **74**, 054406 (2006).

[34] C. Frontera, J. L. García-Muñoz, A. E. Carrillo, C. Ritter, D. M. Marero, and A. Caneiro, Phys. Rev. B **70**, 184428 (2004).

[35] Z. Henkie, P. J. Markowski, A. Wojakowski, and Ch. Laurent, J. Phys. E: Sci. Instrum. **20**, 40 (1987).

[36] Z. Henkie and R. Wawryk, Solid State Commun. **122**, 1 (2002).

[37] J. Wosnitza, A. D. Bianchi, J. Freudenberger, J. Haase, T. Herrmannsdoerfer, N. Kozlova, L. Schultz, Y. Skourski, S. Zherlitsyn, and S. A. Zvyagin, J. Magn. Magn. Mater. **310**, 2728 (2007).

[38] N. Kozlova, M. Kozlov, D. Eckert, K.-H. Müller, and L. Schultz, J. Magn. Magn. Mater. **272-276**, 1679 (2004).

[39] D. Eckert, R. Grössinger, M. Dörr, F. Fisher, A. Handstein, D. Hinz, H. Siegel, P. Verges, and K.-H. Müller, Phys. B: Condens. Matter **294-295**, 705 (2001).

[40] N. F. Mott and E. A. Davis, *Electronic Processes in Non-Crystalline Materials*, 2nd ed., (Clarendon Press, Oxford, 1979), pp. 45–46.

[41] N. F. Mott and W. D. Twose, Adv. Phys. **10**, 107 (1961).

[42] P. J. Markowski, Z. Henkie, and A. Wojakowski, Solid State Commun. **32**, 1119 (1979).

[43] R. E. Baumbach, P. C. Ho, T. A. Sayles, M. B. Maple, R. Wawryk, T. Cichorek, A. Pietraszko, and Z. Henkie, PNAS **105**, 17307 (2008).

[44] P. S. Riseborough, Phys. Rev. B **68**, 235213 (2003).

[45] H. Ikeda and K. Miyake, J. Phys. Soc. Jpn. **65**, 1769 (1996).

[46] T. A. Sayles, R. E. Baumbach, W. M. Yuhasz, M. B. Maple, Ł. Bochenek, R. Wawryk, T. Cichorek, A. Pietraszko, Z. Henkie, and P. C. Ho, Phys. Rev. B **82**, 104513 (2010).

[47] M. Očko, C. Gaibel, and F. Steglich, Phys. Rev. B **64**, 195101 (2001).

[48] F. J. Blatt, *Physics of Electronic Conduction in Solids* (McGraw-Hill, New York, 1968).

[49] I. P. Zvyagin, Phys. Status Solidi B **58**, 443 (1973); M. Pollak and B. I. Shklovskii, (North Holland, Amsterdam, 1991), p.143.

[50] H. Overhof, Phys. Status Solidi B **67**, 709 (1975).

[51] E. S. Vlakhov, R. A. Chakalov, R. I. Chakalova, K. A. Nenkov, K. Dörr, A. Handstein, and K. H. Müller, J. Appl. Phys. **83**, 2152 (1998).

[52]K. Dörr, K. H. Müller, E. S. Vlakhov, R. A. Chakalov, R. I. Chakalova, K. Nenkov, A. Holtzapfel, and L. Schultz, J. Appl. Phys. **83**, 7079 (1998).
[53]E. S. Vlakhov, K. Dörr, K. H. Müller, K. A. Nenkov, A. Handstein, T. Walter, R. A. Chakalov, R. I. Chakalova, T. I. Donchev, and A. Y. Spasov, Vacuum **58**, 404 (2000).
[54]K. Dörr, J. M. De Teresa, K. H. Müller, D. Eckert, T. Walter, E. Vlakhov, K. Nenkov, and L. Schultz, J. Phys. Condens. Matter **12**, 7099 (2000).
[55]K. Dörr, K. H. Müller, N. Kozlova, P. Reutler, R. Klingeler, B. Büchner, and L. Schultz, J. Magn. Magn. Mater. **290-291**, 416 (2005).
[56]E. S. Vlakhov, K. A. Nenkov, T. I. Donchev, and A. Y. Spasov, Vacuum **69**, 249 (2002).
[57]E. S. Vlakhov, K. A. Nenkov, T. I. Donchev, E. S. Mateev, R. A. Chakalov, A. Szewczyk, M. Baran, and K. Piotrowski, J. Magn. Magn. Mater. **290-291**, 955 (2005).
[58]V. Markovich, E. S. Vlakhov, Y. Yuzhelevskii, B. Blagoev, K. A. Nenkov, and G. Gorodetsky, Phys. Rev. B **72**, 134414 (2005).
[59]V. Markovich, E. S. Vlakhov, Y. Yuzhelevskii, B. Blagoev, K. A. Nenkov, and G. Gorodetsky, Physika Status Solidi (c) **3**, 61 (2006).
[60]H. Y. Hwang, S. W. Cheong, N. P. Ong, and B. Batlogg, Phys. Rev. Lett. **77**, 2041 (1996).
[61]S. Lee, H. Y. Hwang, B. I. Shraiman, W. D. Ratcliff II, and S. W. Cheong, Phys. Rev. Lett. **82**, 4508 (1999).
[62]J. E. Evetts, M. G. Blamire, N. D. Mathur, S. P. Isaac, B. S. Teo, L. F. Cohen, and J. L. Macmanus-Driscoll, Philos. Trans. R. Soc. London A **356**, 1593 (1998).
[63]K. Steenbeck, T. Eick, K. Kirsch, K. O'Donnell, and E. Steinbeiss, Appl. Phys. Lett. **71**, 968 (1997).
[64]P. Gierlowski, A. Szewczyk, A. V. Abal'oshev, E. S. Vlakhov, T. I. Donchev, and B. Blagoev, Acta Phys. Pol. A **106**, 715 (2004).
[65]N. Kozlova, K. Dörr, D. Eckert, T. Walter, and K. H. Müller, J. Magn. Magn. Mater. **261**, 48 (2003).
[66]B. Fisher, K. B. Chashka, L. Patlagan, and G. M. Reisner, J. Magn. Magn. Mater. **272-276**, 1790 (2004).
[67]D. Serrate, J. M. De Teresa, P. A. Algarabel, M. R. Ibarra, and J. Galibert, Phys. Rev. B **71**, 104409 (2005).